Topological Aspects of Symmetry Breaking in Triangular-Lattice Ising Antiferromagnets

Andrew Smerald,[1] Sergey Korshunov,[2,*] and Frédéric Mila[1]
[1]*Institute of Physics, Ecole Polytechnique Fédérale de Lausanne (EPFL), CH-1015 Lausanne, Switzerland*
[2]*L. D. Landau Institute for Theoretical Physics, Kosygina 2, Moscow 119334, Russia*
(Received 4 February 2016; revised manuscript received 21 March 2016; published 9 May 2016)

Using a specially designed Monte Carlo algorithm with directed loops, we investigate the triangular lattice Ising antiferromagnet with coupling beyond the nearest neighbors. We show that the first-order transition from the stripe state to the paramagnet can be split, giving rise to an intermediate nematic phase in which algebraic correlations coexist with a broken symmetry. Furthermore, we demonstrate the emergence of several properties of a more topological nature such as fractional edge excitations in the stripe state, the proliferation of double domain walls in the nematic phase, and the Kasteleyn transition between them. Experimental implications are briefly discussed.

DOI: 10.1103/PhysRevLett.116.197201

The triangular-lattice Ising antiferromagnet (TLIAF) is the archetypal model of frustration. Ground states of the nearest-neighbor (NN) model obey the local constraint that triangles cannot host three equivalent Ising spins, and it follows that there is an extensive entropy [1,2]. This results in a critical state, characterized by algebraic correlations between the spins [3,4].

In reality, interactions are rarely limited to NN, and a more realistic Hamiltonian takes the form

$$\mathcal{H}_{Is} = \sum_{(i,j)} J_{ij}\sigma_i\sigma_j, \tag{1}$$

where $\sigma_i = \pm 1$ and $J_{ij} > 0$. This model is experimentally relevant in a diverse range of systems, including artificial dipolar magnets [5], materials such as $Ba_3CuSb_2O_9$ where electrically charged dumbbells act as Ising degrees of freedom [6,7], trapped ions [8,9], frustrated Coulomb liquids [10], Josephson junction arrays [11], and absorbed monolayers [12].

In spite of its ubiquity, this model has received limited attention. The difficulty in analyzing $\mathcal{H}_{Is}$ [Eq. (1)] arises from the critical nature of the NN ground-state manifold, which is very sensitive to perturbation, and in the presence of further-neighbor coupling the model is not amenable to an analytic solution. Besides, in the limit $J_1 \to \infty$ as compared to the other characteristic energy scales of the problem (J_2, J_3, etc.), Monte Carlo (MC) simulations based on the Metropolis algorithm are unable to reach the ground state, and the problem of freezing remains even when this constraint is relaxed, for example in the case of dipolar interactions [13].

The current understanding of the properties of $\mathcal{H}_{Is}$ is based on estimates of the energy and entropy of different types of extended defects. This results in the prediction that the broken $Z_2 \times Z_3$ symmetry of the low-temperature stripe state [14–16] can be restored either in a single first-order transition, or via a pair of transitions, where the low-temperature, Z_2-restoring transition is second order and the higher-temperature, Z_3-restoring transition is first order [14]. When the transition is split, an intermediate phase of nematic type is revealed, and it is characterized by a set of fluctuating double domain walls [14] (DDWs).

In this Letter, we show that the difficulty in simulating the TLIAF with MC calculations arises from the topological structure of the NN manifold of ground states. This can be

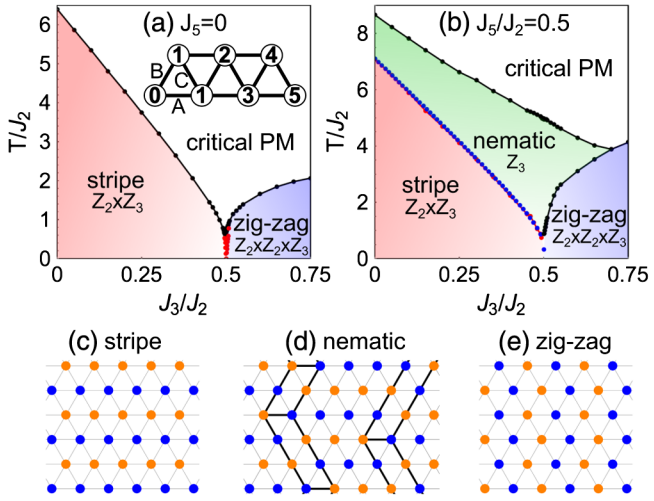

FIG. 1. Representative phase diagrams of the TLIAF with $J_1/T \to \infty$, determined by MC simulation. All phase boundaries were determined from the winding number. (a) In the presence of J_2 and J_3 interactions there are 3 possible phases, and all transitions are first order. (Inset) Illustration of first to fifth neighbors of the central site and bond labeling. (b) In the presence of a J_5 interaction an intermediate nematic state is revealed. Blue (red) dots show the position of a second order Kasteleyn transition calculated analytically [14,17] (with MC calculations). (c) Stripe phase. (d) Nematic phase with fluctuating double domain walls (shown in black). (e) Zig-zag phase.

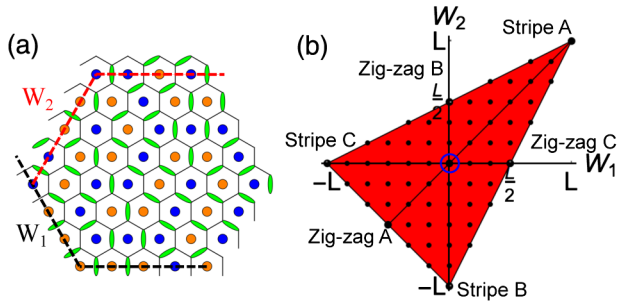

FIG. 2. Winding number sectors of the TLIAF. (a) An Ising configuration within the nearest-neighbor ground state manifold can be mapped onto a dimer covering of the dual honeycomb lattice. The dimer crossings of the reference lines are used to calculate the winding number $W = (W_1, W_2)$. (b) The allowed winding number sectors, illustrated for $L = 12$. The $W = (0, 0)$ sector (circled in blue) has a macroscopic degeneracy, while the sectors containing stripe (zig-zag) states have a two (four)-fold degeneracy.

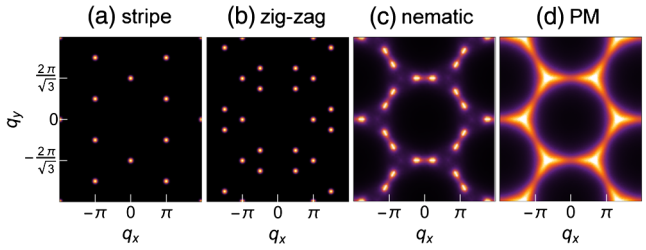

FIG. 3. Representative plots of the structure factor in the 4 phases (see Fig. 1). (a) In the stripe phase there are a set of Bragg peaks, and similarly (b) in the zig-zag phase. (c) The nematic phase is characterized by pairs of peaks, with power-law singularities, and the peak splitting is proportional to the density of double domain walls. (d) The critical paramagnet also has peaks with power-law singularities, but at different positions compared to the nematic state.

resolved by employing a specially designed worm algorithm [17] that allows one to travel through the different topological sectors present in the $J_1 \to \infty$ limit, and by using the topological winding number rather than the order parameters to map out the phase diagrams. The resulting phase diagrams of two representative models (see Fig. 1) are in excellent agreement with the predictions of Ref. [14], including the stabilization of an intermediate nematic phase for large enough fifth-neighbor coupling. We also show that the hidden topological nature of the model leads to a number of new insights, including fractional edge excitations, and the Kasteleyn nature of the phase transition between the stripe and the nematic phases [36].

We start by reviewing the topological properties of the NN ground-state manifold. This can be split into topological sectors by defining a pair of winding numbers $W = (W_1, W_2)$. A useful first step is to map the TLIAF onto a dimer model on the dual honeycomb lattice, in which a dimer is placed on each honeycomb bond that separates two equivalent Ising spins [36] (see Fig. 2). Two reference lines are defined on the triangular lattice and for each honeycomb bond crossing the reference line the associated winding number is augmented by $\mp 1/3$ in the absence of a dimer and $\pm 2/3$ in the presence of a dimer. The sign is determined by defining a direction in which the reference line should be crossed, splitting the honeycomb lattice into two interpenetrating sublattices 1 and 2 and taking the upper sign if the bond direction is $1 \to 2$ and the lower sign for $2 \to 1$. The NN manifold is dominated by the $W = (0, 0)$ sector, and in the thermodynamic limit the ratio of configurations in this sector compared to the total number of configurations tends to 0.996 [17].

Let us now consider the effect of further-neighbor couplings on this degenerate ground state manifold (or equivalently the limit $J_1 \to \infty$). A positive J_2 selects three stripe states which belong to the topological sector $W = (L, L)$ for stripes parallel to A bonds, $W = (0, -L)$ for B stripes and $W = (-L, 0)$ for C stripes. These topological sectors are as far as possible from the dominant sector $W = (0, 0)$, and up to the Z_2 degeneracy associated with global spin flips, they contain only these states (see Fig. 2). The situation is similar for the zig-zag ground states realized for $J_3/J_2 > 1/2$ [17]. Starting from high temperature, these states are thus out of reach of a single spin flip algorithm. So we have developed a sophisticated worm algorithm with nonlocal updates that allow the system to change topological sector. Such updates involve identifying loops of alternating dimer-covered and empty bonds, and exchanging the two, thus flipping all the spins contained within the loop [18]. In addition, we found that it was necessary in practice to direct the creation of the loops using all further-neighbor interactions, and this results in rejection-free updates [17].

To map out the phase diagram of the models with $J_1 \to \infty$, the most efficient way was to keep track of the nonanalyticities of the temperature dependent winding number defined by $W_{\max} = \max(|W_1|, |W_2|, |W_2 - W_1|)$. Including only J_2 and J_3, the resulting phase diagram consists of three phases: a high temperature paramagnetic phase, and two low-temperature ordered phases, a stripe phase for $J_3/J_2 < 1/2$, and a zig-zag phase for $J_3/J_2 > 1/2$. The general phase diagram can potentially include an additional intermediate phase of nematic character, as shown in Fig. 1 for $J_5/J_2 = 0.5$. The nature of the various phases can be revealed by looking at snapshots [17]. A more precise characterization of direct experimental relevance is provided by the structure factor $S(\mathbf{q}) = \sum_{ij} \langle \sigma_i \sigma_j \rangle e^{i\mathbf{q}\cdot\mathbf{r}}$, with $\mathbf{r} = \mathbf{r}_i - \mathbf{r}_j$. Simulations are shown in Fig. 3. The ordered phases have Bragg peaks, while the nematic phase has power-law singularities.

We next discuss in more detail the various phases, starting with the stripe phase. This simple looking structure has remarkable properties. First, the state is fluctuationless

at all T. Local excitations involve the creation of pairs of defect triangles, with an energy cost of $4J_1$, while nonlocal excitations involve the formation of DDW excitations that wind the system [14], with an energy cost proportional to J_2L. Both of these types of excitations are excluded, the local ones due to the condition $J_1 \to \infty$ and the nonlocal ones by taking the thermodynamic limit $L \to \infty$. The zigzag phase has very similar properties. However, the stripe state does support fractional edge excitations that are energetically forbidden from penetrating the bulk. We have performed simulations with open boundary conditions in order to study these [17], and a representative configuration is shown in Fig. 4. For boundaries orientated parallel to the stripe direction, defect triangles can be created without a J_1-energy cost. In fact they require an energy of only $2J_2 - 8J_3 + 4J_4$, and thus there will be a thermally activated population. Since, in the bulk, defect triangles are constrained to appear in pairs, these are fractional excitations. Local dynamics allows these defect triangles to propagate freely along the boundary, but penetration into the bulk is penalized by an energy cost proportional to the penetration depth.

The intermediate nematic state involves the proliferation of DDW defects (see Fig. 1). The DDWs run perpendicular to the direction of the stripes and therefore the nematic state breaks the sixfold rotational symmetry of the triangular lattice down to a twofold symmetry. The state is best characterized by the density of the DDWs, $\nu(T)$, and this is related to the winding number according to $\nu(T) = 4(L - W_{\max})/3L$. It can be seen in Fig. 5 that $W_{\max}$ varies continuously with temperature. The DDWs do not form a periodic arrangement but instead fluctuate, and the state is critical.

The critical nature of the nematic state can be demonstrated by studying the peaks of the structure factor, $S(\mathbf{q})$. We find that $S(\mathbf{q}_{\text{peak}} + \delta q) \propto |\delta \mathbf{q}|^{\tau-2}$, where τ is a temperature-dependent critical exponent. This results in algebraic correlations according to $S(\mathbf{r}) = \langle \sigma_i \sigma_j \rangle \propto r^{-\tau}$, and in the direction perpendicular to the walls one can write $S(\mathbf{r}) \propto \cos(\pi r/L)(L/r)^{\tau}$. Simulations show that $0 < \tau < 1/2$, and it is demonstrated below that $\tau = 1/2$ close to T_{DDW}.

Next we turn to the nature of the phase transitions. For $J_5 = 0$ the transition out of the stripe state is first order, and involves an abrupt change of the winding number sector. This can be seen in Fig. 5, where in the stripe state $W_{\max} = L$, while in the critical paramagnet $W_{\max} \to 0$. For $J_5 \neq 0$ the high-temperature transition from the nematic state to the critical paramagnet is also first order, and involves a transition from an intermediate winding number sector to $W_{\max} \to 0$.

More interesting is the low-temperature second-order transition that occurs in the presence of a J_5 interaction (see Fig. 5). At this phase transition the Ising Z_2 symmetry is broken, and thus one would naively expect that the transition is in the Ising universality class. However, if one constructs an order parameter based on this symmetry it exhibits a discontinuous jump at the transition. Furthermore, if one makes a mapping to a dimer model on the honeycomb lattice, the transition remains unchanged, despite the fact that the Z_2 symmetry has been discarded. In fact it is the change of topology and not of symmetry that drives the transition and it is within the Pokrovsky-Talapov universality class [19,20].

The best way to characterize this transition is as a nonanalyticity in the winding number, $W_{\max}$, and therefore a divergence of the associated susceptibility. This occurs at T_{DDW}, which can be calculated exactly and is the temperature at which the free-energy of a DDW excitation vanishes [14,17]. The second-order nature of the transition

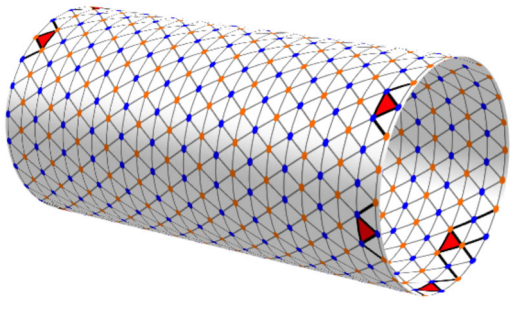

FIG. 4. Fractional edge excitations in the low-temperature stripe state. While the stripe state is fluctuationless in the bulk, defect triangles (red) can be created at open boundaries at an energy cost of $2J_2 - 8J_3 + 4J_4$. The snapshot shown is taken from a Monte Carlo simulation of the $J_1 - J_2$ model performed on a cylinder at $T = 1.5J_2$ (for comparison $T_1 = 6.39J_2$).

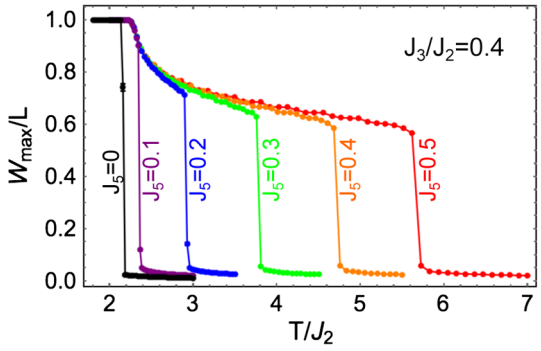

FIG. 5. Temperature dependence of the winding number with $J_2 = 1$, $J_3 = 0.4$ and variable J_5. Monte Carlo simulations on an $L = 96$ cluster are used to measure $W_{\max} = \max(|W_1|, |W_2|, |W_2 - W_1|)$, and errors are typically smaller than the point size. For $J_5 = 0$ (black) there is a direct first order phase transition from the low-temperature stripe state ($W_{\max} = L$) to the high-temperature critical paramagnet ($W_{\max} \to 0$). For all other values of J_5 there is a second order phase transition at $T_{\text{DDW}} = 2.29$ between the stripe state and a nematic state (variable $W_{\max}$), followed by a first order transition to the critical paramagnet at higher T.

is ensured by the noncrossing constraint of the DDWs, which leads to an entropically driven repulsion [19,20].

In order to achieve a quantitative understanding of the critical behavior, it is useful to make a mapping to a 1D quantum model of fermions [17,19–21]. A DDW can be identified with a fermion whose imaginary time propagation is parallel to the wall, and the noncrossing condition is encoded in the fermionic anticommutation relation. The fermionic chemical potential, μ, is related to the temperature of the classical model by $\mu \propto T - T_{\mathrm{DDW}}$. In the fermionic language, the second-order phase transition between the nematic and stripe states is a metal-insulator transition. Close to this transition the density of fermions will be very low, and therefore one can ignore fermion-fermion interactions, which become progressively more important at higher temperatures. In consequence one finds $\nu(T) \propto (T - T_{\mathrm{DDW}})^{\beta}$, with $\beta = 1/2$. This critical exponent is typical of the Pokrovsky-Talapov universality class [19,20], and is clearly not typical of an Ising transition. A similar analysis of the structure factor leads to the prediction $\tau = 1/2$ close to the transition [21]. We have confirmed these predictions by MC simulation [17].

If the $J_1 \to \infty$ constraint is relaxed, then for $T > 0$ there will be a low but finite density of defect triangles in the bulk of the stripe state. These have to be created in pairs, and are confined since they are joined by a pair of DDWs, and thus the free energy cost grows linearly with their separation [17]. In contrast, defect triangles are deconfined in the nematic state since the free energy of DDWs goes to zero on entering the state. In fact, if one of the defect triangles winds around the system, and then the pair annihilates, a pair of DDWs has been created. We expect that the relaxation of the $J_1 \to \infty$ constraint will cause this transition to cross over to the Ising universality class, but this will only be physically significant in an exponentially suppressed temperature window [22,37,38]. Thus, unless J_1 is small, the behavior remains dominated by the Kasteleyn character of the $J_1 \to \infty$ limit.

It is useful to compare and contrast the present findings with those in related systems. First, a number of states with a similar coexistence of order and liquidity, as in the nematic state, have recently been found in other frustrated magnets [39–45]. There are also close parallels with the floating phases found in systems of gases adsorbed onto a substrate [23]. The transition between the stripe and nematic phases has a lot in common with the Kasteleyn model of dimers on the honeycomb lattice [36] and with spin ice in a [100] magnetic field, which displays a 3D Kasteleyn transition [24,25,46]. In particular, the second-order transition that we find in the presence of a J_5 interaction is within the same Pokrovsky-Talapov universality class as Kasteleyn's model. However, there are a number of important differences. The model we study is isotropic and therefore the rotational lattice symmetry is broken spontaneously, rather than in the Hamiltonian. This isotropy leads to a topological degeneracy in the ground state and the possibility of an intermediate nematic phase. Also, the Z_2 symmetry associated with the Ising spins is not present in the Kasteleyn model, and this leads to the existence of fractional edge states, as well as defect triangles in the bulk when the $J_1 \to \infty$ constraint is relaxed. The closest analogue to the physics we present here is probably spin ice with a uniaxial distortion and a 4-spin interaction [44]. In this case the 4-spin interaction splits a single first-order transition into two second-order transitions. However, the uniaxial distortion breaks most of the symmetry of the pyrochlore lattice by hand, and the physical interpretation of strings is different from the DDWs of the TLIAF.

Finally, let us discuss in what circumstances the transition can be expected to be split. In Fig. 1 we have ignored J_4 interactions, since this acts against the J_5-induced splitting of the transition by reducing the temperature of the first-order line [14]. Similar reasoning can be extended to further-neighbor couplings and for a set of interactions that decrease smoothly with distance we expect that a single first-order transition is typical. We have checked that this is the case for long-range dipolar interactions. However, the magnetic exchange interaction does not necessarily lead to couplings that decay smoothly with separation, and can therefore result in systems where the transition is split.

To show that this is a generic possibility, we have derived a general condition by mapping the Ising degrees of freedom onto height configurations of the [111] face of a crystal with a simple cubic lattice [26]. A continuum free energy can thus be written as [14,17],

$$\mathcal{F}[h] = \int d^2r \left\{ \frac{K_2}{2}(\nabla h)^2 + K_3 \prod_{\alpha} (\mathbf{e}_\alpha \cdot \nabla) h + \frac{K_4}{4}(\nabla h)^4 - V_0 \cos\left[\frac{2\pi}{3}(h_{\mathrm{str}} - h) \right] \right\}, \quad (2)$$

where K_2 is temperature dependent, K_3 is related to the energy cost of double domain walls, K_4 ensures that the free energy is bounded from below, and the last term is a locking potential that favours integer values of the height field. Here $h_{\mathrm{str}}(\mathbf{r})$ is the height configuration in one of the stripe states and $\mathbf{e}_\alpha$ is a set of 3 unit vectors forming 120° angles with one another. Analysis of this model shows that the transition is split when [17],

$$\frac{K_3^2}{8K_4} > \frac{144 V_0}{\pi^4 [|\nabla h_{\mathrm{str}}| - K_3/(2K_4)]^2}. \quad (3)$$

In conclusion, we have shown that the physics of the extended TLIAF with large nearest-neighbor coupling, a model of direct relevance in several contexts, is remarkably rich, with a phase diagram that can only be properly understood by invoking both broken symmetry and

topological concepts. Indeed, while all phases can be characterized by their broken symmetry, several of their properties are more topological in nature, such as the fluctuationless character of the low-temperature stripe state and its fractional edge excitations, the proliferation of double-domain walls in the intermediate nematic phase that appears when the first-order transition is split by, for example, a fifth-neighbor interaction, and the Kasteleyn transition that separate these phases. Far from being of pure academic interest, the topological aspects of the problem might actually be the key to understanding the properties of systems in which the development of true symmetry breaking is hampered by a purely local dynamics, or by the finite size of the sample. For instance, finite clusters are expected to develop domain walls to minimize their edge energy if they can reach their ground states, or to support edge excitations if they cannot. We hope that the present Letter will motivate experimental studies along these lines.

We are grateful to Ludovic Jaubert for a useful discussion. We also thank the Swiss National Science Foundation and its SINERGIA network "Mott physics beyond the Heisenberg model" for financial support. We sadly regret the untimely death of one of our co-authors, Sergey Korshunov, shortly before this Letter was completed.

[*] Deceased.

[1] G. H. Wannier, Phys. Rev. **79**, 357 (1950).
[2] R. M. F. Houtappel, Physica **16**, 425 (1950).
[3] J. Stephenson, J. Math. Phys. (N.Y.) **5**, 1009 (1964).
[4] J. Stephenson, J. Math. Phys. (N.Y.) **11**, 413 (1970).
[5] E. Mengotti, L. J. Heyderman, A. Bisig, A. Fraile Rodríguez, L. Le Guyader, F. Nolting, and H. B. Braun, J. Appl. Phys. **105**, 113113 (2009).
[6] S. Nakatsuji, K. Kuga, K. Kimura, R. Satake, N. Katayama, E. Nishibori, H. Sawa, R. Ishii, M. Hagiwara, F. Bridges, T. U. Ito, W. Higemoto, Y. Karaki, M. Halim, A. A. Nugroho, J. A. Rodriguez-Rivera, M. A. Green, and C. Broholm, Science **336**, 559 (2012).
[7] A. Smerald and F. Mila, Phys. Rev. Lett. **115**, 147202 (2015).
[8] J. W. Britton, B. C. Sawyer, A. C. Keith, C. C. J. Wang, J. K. Freericks, H. Uys, M. J. Biercuk, and J. J. Bollinger, Nature (London) **484**, 489 (2012).
[9] C. Senko, J. Smith, P. Richerme, A. Lee, W. C. Campbell, and C. Monroe, Science **345**, 430 (2014).
[10] S. Mahmoudian, L. Rademaker, A. Ralko, S. Fratini, and V. Dobrosavljević, Phys. Rev. Lett. **115**, 025701 (2015).
[11] S. E. Korshunov, Phys. Rev. Lett. **94**, 087001 (2005).
[12] J. Villain and M. Gordon, Surf. Sci. **125**, 1 (1983).
[13] U. K. Rößler, J. Appl. Phys. **89**, 7033 (2001).
[14] S. E. Korshunov, Phys. Rev. B **72**, 144417 (2005).
[15] B. Metcalf, Phys. Lett. **46A**, 325 (1974).
[16] M. Kaburagi and J. Kanamori, Jpn. J. Appl. Phys. **13**, 145 (1974).
[17] See Supplemental Material at http://link.aps.org/supplemental/10.1103/PhysRevLett.116.197201 for further information concerning winding number sectors, the Monte Carlo worm algorithm, the phase diagram, the transition temperature T_{DDW}, the second-order phase transition between the stripe and nematic states, the role of defect triangles, and the analysis of a height model to understand the splitting of the transition. This includes Refs. [1,14,18–35].
[18] W. Zhang, T. M. Garoni, and Y. Deng, Nucl. Phys. **B814**, 461 (2009).
[19] V. L. Pokrovsky and A. L. Talapov, Phys. Rev. Lett. **42**, 65 (1979).
[20] V. L. Pokrovsky and A. L. Talapov, Zh. Eksp. Teor. Fiz. **78**, 269 (1980).
[21] J. Villain and P. Bak, J. Phys. (Paris) **42**, 657 (1981).
[22] H. J. Schulz, B. I. Halperin, and C. L. Henley, Phys. Rev. B **26**, 3797 (1982).
[23] P. Bak, Rep. Prog. Phys. **45**, 587 (1982).
[24] L. D. C. Jaubert, J. T. Chalker, P. C. W. Holdsworth, and R. Moessner, Phys. Rev. Lett. **100**, 067207 (2008).
[25] S. Powell and J. T. Chalker, Phys. Rev. B **78**, 024422 (2008).
[26] H. W. J. Blote and H. J. Hilborst, J. Phys. A **15**, L631 (1982).
[27] O. F. Syljuåsen and A. W. Sandvik, Phys. Rev. E **66**, 046701 (2002).
[28] A. W. Sandvik and R. Moessner, Phys. Rev. B **73**, 144504 (2006).
[29] F. Alet, Y. Ikhlef, J. L. Jacobsen, G. Misguich, and V. Pasquier, Phys. Rev. E **74**, 041124 (2006).
[30] J. Glosli and M. Plischke, Can. J. Phys. **61**, 1515 (1983).
[31] T. Takagi and M. Mekata, J. Phys. Soc. Jpn. **64**, 4609 (1995).
[32] E. Rastelli, S. Regina, and A. Tassi, Phys. Rev. B **71**, 174406 (2005).
[33] C. S. O. Yokoi, J. F. Nagle, and S. R. Salinas, J. Stat. Phys. **44**, 729 (1986).
[34] Y. Jiang and T. Emig, Phys. Rev. B **73**, 104452 (2006).
[35] S. Powell and J. T. Chalker, Phys. Rev. B **80**, 134413 (2009).
[36] P. W. Kasteleyn, J. Math. Phys. (N.Y.) **4**, 287 (1963).
[37] T. Bohr, Phys. Rev. B **25**, 6981 (1982).
[38] S. B. Rutkevich, J. Phys. A **30**, 3883 (1997).
[39] G.-W. Chern, P. Mellado, and O. Tchernyshyov, Phys. Rev. Lett. **106**, 207202 (2011).
[40] A. F. Albuquerque, F. Alet, and R. Moessner, Phys. Rev. Lett. **109**, 147204 (2012).
[41] R. A. Borzi, D. Slobinsky, and S. A. Grigera, Phys. Rev. Lett. **111**, 147204 (2013).
[42] P. C. Guruciaga, S. A. Grigera, and R. A. Borzi, Phys. Rev. B **90**, 184423 (2014).
[43] M. E. Brooks-Bartlett, S. T. Banks, L. D. C. Jaubert, A. Harman-Clarke, and P. C. W. Holdsworth, Phys. Rev. X **4**, 011007 (2014).
[44] S. Powell, Phys. Rev. B **91**, 094431 (2015).
[45] L. D. C. Jaubert, SPIN **05**, 1540005 (2015).
[46] T. Fennell, O. A. Petrenko, B. Fåk, J. S. Gardner, S. T. Bramwell, and B. Ouladdiaf, Phys. Rev. B **72**, 224411 (2005).